WELDING RESEARCH

SUPPLEMENT TO THE *WELDING JOURNAL,* JULY 2008
Sponsored by the American Welding Society and the Welding Research Council

Liquation of Mg Alloys in Friction Stir Spot Welding

The susceptibility of Mg alloys to liquid formation and cracking in FSSW and methods to test and explain the susceptibility of Mg and Al alloys are demonstrated

BY Y. K. YANG, H. DONG, H. CAO, Y. A. CHANG, AND S. KOU

ABSTRACT. The use of friction stir spot welding (FSSW) to join Al alloys in automobiles (e.g., by Mazda Motors) is expected to extend to Mg alloys in view of their increasing use to further reduce the vehicle weight. FSSW is considered a solid-state welding process, but liquation (liquid formation) and cracking have been reported recently in Mg alloys in FSSW. In the present study, liquation in Mg alloys was investigated using as-cast AZ91E Mg (~Mg-8.6Al-0.6Zn, a widely used Mg alloy) as an example and 6061-T6 Al (~Al-1Mg-0.6Si, an Al alloy widely welded by FSSW) as a reference for comparison. With the same welding schedule, liquation occurred in AZ91E Mg but not 6061 Al. A simple test with an augmented torque to amplify the difference in the liquation susceptibility between different alloys was demonstrated. It showed no liquation in 6061 Al but severe liquation and cracking in AZ91E Mg, including formation of eutectic liquid films, cracking along liquated grain boundaries, removal of liquated material by the tool, and a mirror-like weld top surface. The microstructural evolution leading to liquation in FSSW was presented. Liquation made the torque fluctuate and fail to show a clear peak as the rotating tool shoulder reached and penetrated the workpiece surface. The heat input, determined from the torque and the axial force, was much less with AZ91E Mg than 6061 Al and thus not why AZ91E Mg liquated more severely. A method to explain the liquation susceptibility was thus proposed. The curves of temperature vs. fraction solid (T-f_S) during solidification were calculated. They indicated little liquation-causing constituent in 6061 Al but much more in AZ91E Mg, AM60 Mg, and AZ31 Mg and with a much lower liquation temperature. Most Mg alloys including these three have Al as the major alloying element, thus providing γ (a Mg-Al compound) to react with α (the Mg-rich phase) and cause liquation by the eutectic reaction $\alpha + \gamma \rightarrow L$ at a low temperature ($\leq$ 437°C). The effect of heat treating before welding on liquation in FSSW was discussed.

Y. K. YANG and H. CAO are graduate students and Y. A. CHANG and S. KOU are professors, Department of Materials Science and Engineering, University of Wisconsin, Madison, Wis. H. DONG is lecturer, School of Materials Science and Engineering, Dalian University of Technology, Dalian, China.

Introduction

Since magnesium (Mg) is about one-third lighter than aluminum (Al), the use of Mg alloys in automobiles is expected to rise rapidly in view of the increasing demand to reduce the vehicle weight in order to improve the fuel efficiency and reduce air pollution. The gas tungsten arc welding (GTAW) process can join Mg alloys satisfactorily, but this process is impractical for the automotive industry. The gas metal arc welding (GMAW) process is much more useful, but severe spatter and porosity often occur in GMAW of Mg alloys. Thus, solid-state welding is an attractive alternative for joining Mg alloys.

Friction stir welding (FSW) is a solid-state welding process invented by The Welding Institute in 1991 (Ref. 1). It has been widely used for welding soft materials such as Al and Mg alloys since then. In FSW the pin at the bottom of a rotating cylindrical tool is plunged into a rigidly held workpiece and traversed along the joint to be welded. Welding is achieved by plastic flow of frictionally heated material from ahead of the pin to behind it. In friction stir spot welding (FSSW), as illustrated in Fig. 1, the rotating tool is also plunged into a rigidly held workpiece but without being traversed along any direction. Welding is achieved by plastic flow of frictionally heated material around the pin. A keyhole is left in the workpiece after the tool is withdrawn at the end of FSW or FSSW. FSSW has recently replaced resistance spot welding in making aluminum rear doors in Mazda RX8 passenger cars.

In FSW the tool travels along the joint and the heat input is distributed along the joint. Liquation, that is, formation of liquid, is unlikely to occur in FSW. Cao and Kou (Ref. 2) found no liquation in FSW of 2219 Al. However, in FSSW the tool remains at one spot, where the heat input dwells. Thus, liquation is much more likely to occur.

Gerlich, Yamamoto, North et al. (Refs. 3–7) have recently conducted temperature measurements in FSSW. They embedded thermocouples in a stationary alloy-steel tool to measure temperatures in a rotating workpiece at the surfaces of the tool shoulder and pin. Temperatures approaching or exceeding the liquation temperature have been measured in Mg alloys including AZ91 Mg extrusions and AM60 Mg sheets prepared by thixomolding (a casting process), wrought AZ31 Mg sheets (Refs. 4, 5), and aerospace Al alloys including 2024 Al and 7075 Al (Ref. 6). Microstructural evidence of liquation was observed in the resultant welds. Thus, liquation can occur in FSSW even though

KEYWORDS

Cracking
Friction Stir Welding
Friction Stir Spot Welding
Liquation
Magnesiun Alloys
Solid-State Welding

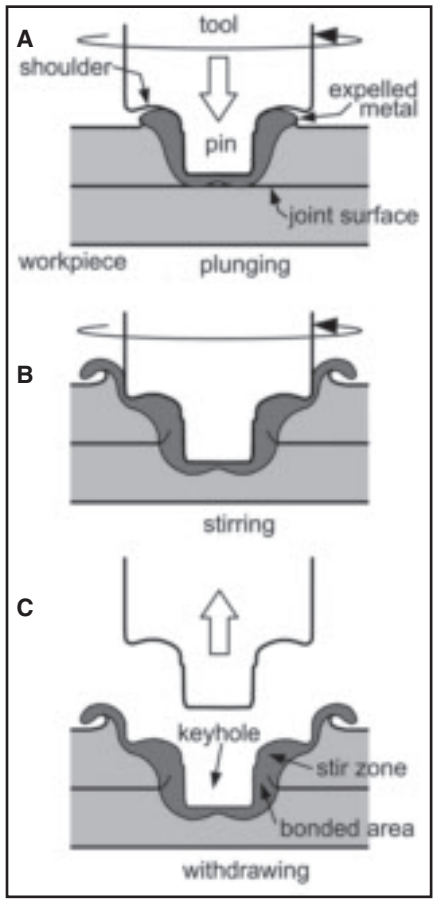

Fig. 1 — Friction stir spot welding (FSSW). A — Plunging; B — stirring; C — withdrawing.

FSSW has been considered as a solid-state welding process. However, 6061 Al, a common Al alloy widely welded by FSW and FSSW, was not found to liquate in FSSW (Ref. 7).

Gerlich (Ref. 7) determined the strain rate of the material adjacent to the rotating tool based on EBSD (electron backscattered diffraction). In both the 2024 Al and 7075 Al, the stain rate dropped sharply above a high rotation speed, e.g., 1500 rev/min. This was attributed to tool slippage caused by liquation.

Liquation, if it occurs in FSSW, can interfere with plastic deformation, degrade the weld quality, and even cause cracking. The high plasticity of the material in FSW has been attributed to the very fine grains produced by dynamic recrystallization caused by the intense plastic deformation associated with the movement of material around the pin and friction heating (Refs. 8, 9). FSSW is expected to be similar in this respect. The presence of liquid films can interfere with plastic deformation. More importantly, it can weaken the stir zone and cause it to crack under the torque of the tool. A liquid-penetration-induced (LPI) cracking mechanism of the following sequence was proposed by Yamamoto et al. (Refs. 4, 5) for cracking in AZ91 Mg during FSSW: 1) formation of liquid eutectic films in the periphery of the stir zone, 2) engulfment of liquid eutectic films by the growing stir zone, 3) penetration of the α (Mg) grain boundaries in the stir zone extremity by the liquid eutectic, and 4) crack propagation along the liquated grain boundaries under the torque of the rotating tool. Even without cracking, the eutectic liquid films become brittle after solidification and can thus reduce the ductility and strength of the weld. Kou and coworkers (Refs. 10–16) have shown liquation-induced cracking in the partially melted zone (PMZ) of Al arc welds and the severe loss of ductility and strength of the PMZ even in the absence of cracking. Various liquation mechanisms in Al arc welds have been discussed by Kou (Ref. 17).

Mg is very similar to Al in many ways, such as low density, low melting point, a soft material weldable by FSSW with an alloy-steel tool, etc. Thus, one may assume that welding schedules good for common Al alloys can automatically be applied to Mg alloys. However, as will be shown in the present study, Mg alloys can be much more susceptible to liquation in FSSW than 6061 Al, and a welding schedule good for 6061 Al may in fact cause liquation in Mg alloys.

The present study investigates the susceptibility of Mg alloys to liquation in FSSW using as-cast AZ91E Mg as an example and 6061 Al as a reference for comparison.

Experimental Procedure

Welds Made without Augmented Torque

6061 Al was welded in the as-received condition of T6, which stands for solution heat treating and artificial aging (Ref. 18). AZ91E Mg was welded in the as-cast condition. The compositions of the alloys used are listed in Table 1.

For both materials the workpiece was 3.1 mm thick and 64 × 44 mm in area. Spot-on-plate welding was conducted, which is equivalent to lap welding two pieces of 1.5-mm sheets. The tool, prepared from H13-steel, had a shoulder of 10-mm diameter and a threaded pin of 4-mm diameter at the top but tapered down at 10 deg along its 1.8-mm length. This tool will be called the 10-mm-shoulder tool hereafter. The rotation speed was 1000 or 1200 rev/min, counterclockwise when viewed from above. The plunge rate was about 0.2 mm/s and the dwell time 4 s.

Welds Made with Augmented Torque

To amplify the difference in the liquation tendency between different alloys, a liquation-susceptibility test was adopted in which the torque was augmented by using a relatively large tool for FSSW. This is similar to amplifying solidification cracking in fusion welds in Varestraint testing (Ref. 19), in which an augmented tensile strain is applied during welding to cause the solidifying weld metal to crack. The tool for welding was an H13-steel tool, with a shoulder of 15-mm diameter and a threaded pin of 5.5-mm diameter and 5.1-mm length beyond the bottom of the shoulder. This tool, shown in Fig. 2, will be called the 15-mm-shoulder tool hereafter. It was originally designed by Friction Stir Link, Inc., Menomonee Falls, Wis., for FSW of 6-mm-thick Al alloys. However, it was found ideal for testing and comparing the liquation tendency in FSSW. As will be shown subsequently, at a 1000-rev/min tool rotation speed, significantly different extents of liquation can be easily induced in different alloys for comparing the liquation susceptibility. A workpiece 6 mm and thicker can be used, depending on availability. The AZ91E Mg workpiece available was 51 × 44 × 9.4 mm and the 6061 Al workpiece was 51 × 51 × 9.7 mm.

The tool rotation speed was 1000 rev/min, counterclockwise when viewed from above. The plunge rate was 0.15 mm/s and the dwell time 4 s. After each weld was made, the tool was plunged into a separate piece of 6061 Al to clean off the AZ91E Mg stuck to the tool during welding. Unlike AZ91E Mg, 6061 Al did not stick to the tool after welding.

Measurements of Torque and Axial Force

To measure the torque and axial force during FSSW, a HAAS TM1 CNC milling machine (5.5 kW or 7.5 hp) equipped with a Kistler Type 9271A dynamometer was used. The dynamometer was cylindrical in shape, and it allowed both the moment acting about its axis and the force parallel to its axis to be measured during FSSW.

Table 1 — Compositions of Workpiece Materials (wt-%)

	Si	Cu	Mn	Mg	Cr	Zn	Ti	Fe	Al
6061 Al	0.62	0.28	0.08	0.89	0.19	0.02	0.01	0.52	balance
AZ91E Mg	—	—	0.24	balance	—	0.65	—	—	8.60
AZ31 Mg*				balance		1.0			3.0
AM60 Mg*			0.5	balance					6.0

*Compositions taken from Ref. 7.

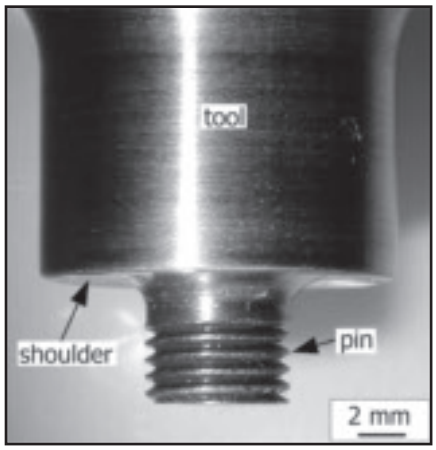

Fig. 2 — Tool with a 15-mm-diameter shoulder for FSSW with augmented torque (tool with a 10-mm-diameter shoulder not shown).

The dynamometer allowed torque measurements in the range of –100 to +100 Nm with a 0.02 Ncm threshold and –1.5 pC/Ncm sensitivity for the torque and force measurements in the range of –5 to +20 kN with a 0.02 N threshold and –1.8 pC/N sensitivity for the axial force. A computer-based data-acquisition system was used to collect the data at 250 Hz and display in real time the curves of torque vs. time and axial force vs. time.

Examination of Weld Microstructure

The resultant welds were cut vertically through the meridian plane, mounted, and polished. Welds of 6061 Al were etched with a solution of 0.5 vol-% HF in water. Welds of AZ91E Mg were etched with an acetic-picric solution consisting of 10 mL acetic acid, 4.2 g picric acid, 10 mL water, and 70 mL ethanol in order to reveal more clearly the fine as well as coarse γ-phase in the SEM image of the base metal. In all other cases, AZ91E Mg welds were polished with a water-based polishing suspension during the final polishing stage and thus etched automatically by the water in the suspension during polishing. Both optical microscopy and scanning electron microscopy (SEM) were used, the latter with the secondary electron mode at 15 kV and a 15-mm working distance. The composition of the intermetallic-compound particles in the alloy was determined by energy dispersive spectroscopy (EDS) to help identify them. Photos of the cross sections of the welds were taken with digital cameras.

Results and Discussion

Welds Made without Augmented Torque

These welds were made on the 3.1-mm-thick workpiece with the 10-mm-shoulder tool at 1000- or 1200- rev/min rotation speed, 0.2 mm/s plunge rate, and the 4-s dwell time. Liquation was observed in the case of AZ91E Mg but not 6061 Al, as will be described as follows. Thus, AZ91E Mg is more susceptible to liquation in FSSW than 6061 Al, and a welding schedule good for 6061 Al can cause liquation in AZ91E Mg.

Figure 3A shows the vertical weld cross section of AZ91E Mg made with 1200 rev/min. The optical micrograph in Fig. 3B shows that dark-etching striations are present near the bottom of the keyhole. As revealed by EDS, these striations are richer in Al than the lighter-etching surrounding areas. This suggests that the striations could have been the thin liquid films that partially dissolved (solutionized) in the α matrix. The SEM image in Fig. 3C shows

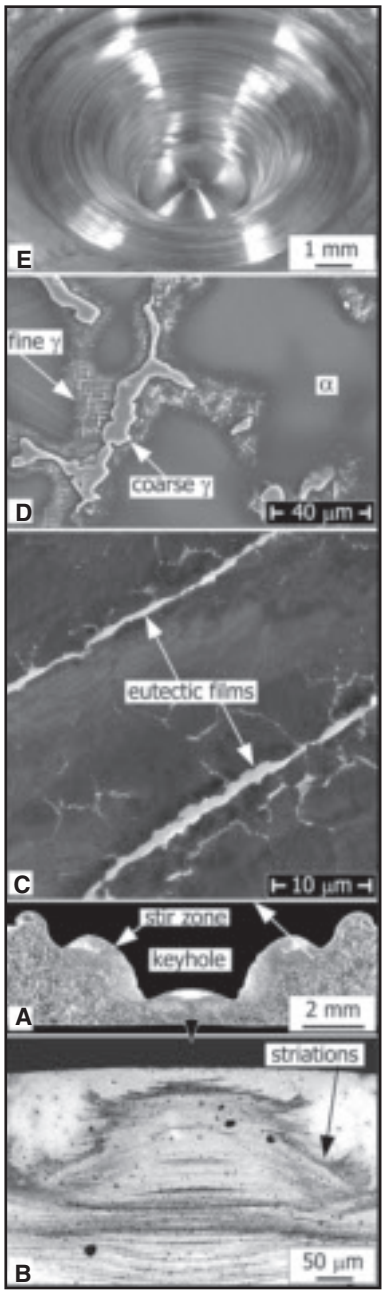

Fig. 3 — Liquation in weld of as-cast AZ91E Mg. A — Vertical cross section; B — optical micrograph showing striations below bottom of keyhole; C — SEM image showing evidence of liquid eutectic films; D — SEM image of base metal; E — weld surface. 10-mm-diameter shoulder, 1200-rev/minrotation speed.

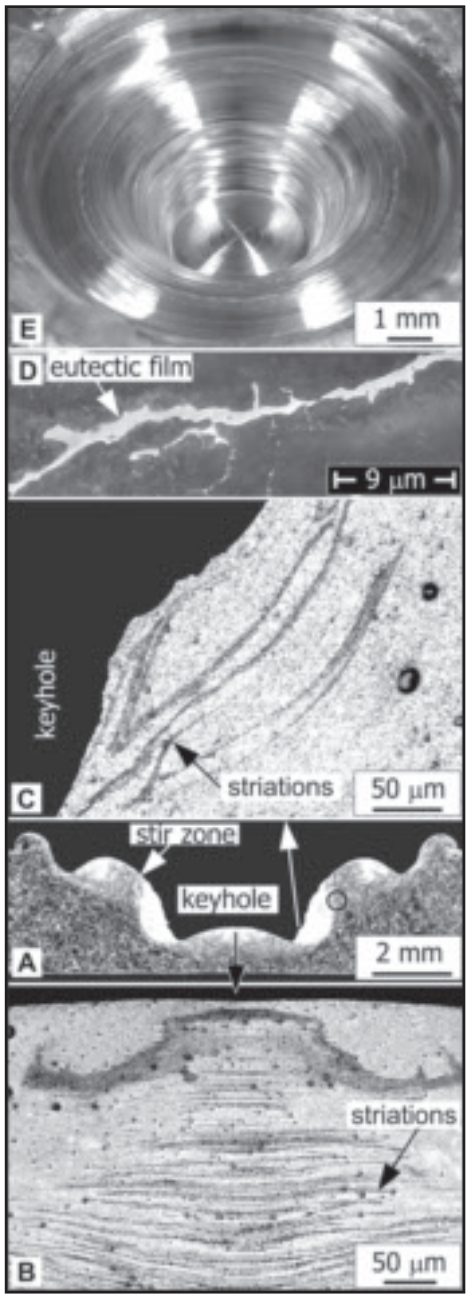

Fig. 4 — Liquation in weld of as-cast AZ91E Mg. A — Vertical cross section; B — optical micrograph showing striations below bottom of keyhole; C — optical micrograph showing striations around bottom of keyhole; D — SEM image showing eutectic film in the area circled in A; E — weld surface. 10-mm-diameter shoulder, 1000-rev/min rotation speed.

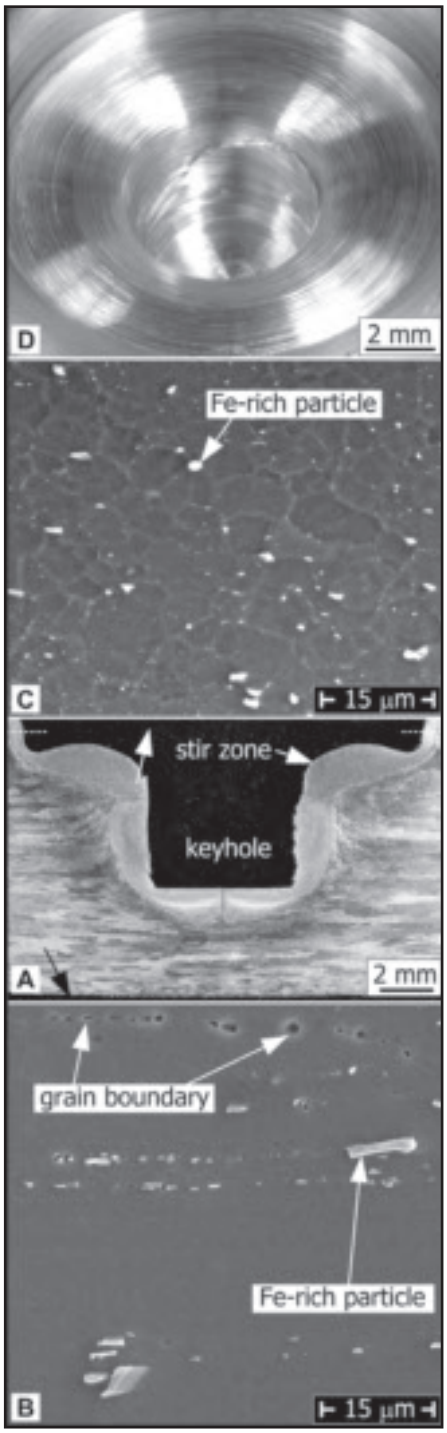

Fig. 5 — No liquation in weld of 6061-T6 Al. A — Vertical cross section; B — SEM image showing base metal microstructure; C — SEM image showing microstructure near weld surface; D — weld surface. 15-mm-diameter shoulder, 1000-rev/min rotation speed.

the evidence of liquid eutectic films in the periphery of the stir zone, with penetration of the liquid eutectic into some grain boundaries near the films. The eutectic films are different in morphology from the eutectic in the base metal. Figure 3D shows the SEM image of the base metal far away from the keyhole. Both coarse and fine γ are found in the eutectic between α dendrite arms (Ref. 20). The former grows from the liquid during casting. The latter grows as precipitation from the supersaturated interdendritic α (Ref. 21). EDS showed that the coarse γ contained about 57 wt-% Mg, 37 wt-% Al, and 4.5 wt-% Zn. The weld top surface (the top surface of the stir zone in contact with the tool shoulder during FSSW) is shown in Fig. 3E. No evidence of liquation is visible on the weld top surface.

Liquation still occurred even when the rotation speed was reduced to 1000 rev/min. The vertical cross section of the resultant weld is shown in Fig. 4A. Figure 4B and C shows dark-etching striations below and around the bottom of the keyhole. Figure 4D shows a eutectic film in the stir zone near its periphery, in the area marked by the circle in Fig. 4A. Thus, liquation occurred near the stir-zone periphery during FSSW. The weld top surface in Fig. 4E again shows no evidence of liquation.

Welds Made with Augmented Torque

These welds were made on the 9.7-mm 6061 Al and 9.4-mm AZ91E Mg with the 15-mm-shoulder tool at 1000-rev/min rotation speed, 0.15-mm/s plunge rate, and 4-s dwell time. The tool shoulder was increased (from 10-mm diameter) to increase the torque and thus amplify the difference in the liquation tendency between different alloys. The welds, as will be shown as follows, revealed no evidence of liquation in 6061 Al but severe liquation and cracking in AZ91E Mg.

6061 Al

No evidence of liquation was observed. Figure 5 shows the 6061 Al spot weld. The vertical cross section of the weld is shown in Fig. 5A. The workpiece surface before welding is indicated by the two short horizontal broken lines in the photo. The pin length was 5.1 mm, and the pin and shoulder penetrated about 5.9 and 0.8 mm, respectively, below the workpiece surface. The base metal microstructure far away from the keyhole is shown by the SEM image in Fig. 5B. The particles are Fe-rich with 20 to 30 wt-% Fe as shown by EDS. These are the Fe-rich intermetallic compounds commonly present in 6061 Al (Ref. 14). Fe is often present in Al alloys as an impurity and it forms Fe-rich particles because of its very low solubility in Al. The holes along the grain boundary are caused by etching, which was heavy in order to bring out the grain structure in the base metal of 6061 Al.

The microstructure of the stir zone near the weld top surface is shown by the SEM image in Fig. 5C. No signs of liquation are evident. No large Fe-rich particles similar to those in the base metal (Fig. 5B) are present here, suggesting they have been broken up by stirring. The grains in the stir zone are much smaller than those in the base metal, suggesting dynamic recrystallization of new small grains in the stir zone. Figure 5D shows the weld top surface. No evidence of liquation can be seen.

AZ91E Mg

Evidence of severe liquation was observed, including formation of liquid eutectic films, cracking along liquated grain boundaries, removal of liquated material by the tool, and a mirror-like weld top surface.

Figure 6 shows the AZ91E Mg spot weld. Figure 6A is the vertical cross section of the weld. The pin and the shoulder penetrated about 5.6 and 0.5 mm, reSpectively, below the workpiece surface. Figure 6B is an optical micrograph showing cracking across in the stir zone and removal of the liquated material from the top of the stir zone. The liquated material stuck to the tool shoulder and was removed by it when the tool was withdrawn at the end of FSSW. The small and large rectangles indicate the locations of Figs. 7 and 8A to be shown subsequently. The weld top surface is mirror-like as shown in Fig. 6C. This is evidence of liquation in the stir zone during FSSW.

Figure 7 is a SEM image taken in the small rectangle in Fig. 6B. It shows evidence of liquid eutectic films near the periphery of the stir zone during FSSW. Several long eutectic films are present in the lower right quarter of the image. A film is enlarged by the inset. The film is normal eutectic (α + γ, that is, composite-like) where it is thick but divorced eutectic (γ plus an α that is connected to the surrounding α matrix) where it is thin. The recrystallized grains in the α dendrites are somewhat visible. In the lower-right corner of Fig. 7, coarse γ particles are visible between α dendrites. In the upper-left half of the same figure, however, only a eutectic consisting of dark α plus thin γ is visible between α dendrites (which tend to be deformed). This eutectic formed as a result of liquation during FSSW.

Further evidence of liquation and cracking in the AZ91E Mg spot weld is shown by the SEM images in Fig. 8. Figure 8A is a SEM image taken in the large rectangle in Fig. 6B. AN α dendrite (marked with α) that is deformed but still discernible is visible just to the left of point 2 near the mid bottom of the micrograph. More dendrites are visible in the lower-right corner of the micrograph.

Figure 8B is an image of the base metal taken at point 1 in Fig. 8A. Microsegregation (that is, coring) of Al and Zn to the interdendritic areas occurs during casting as indicated by the light gray α in the dendrite arms, the dark gray α and white γ in the interdendritic areas. Both coarse and fine γ are present.

Figure 8C is an image taken at point 2 in Fig. 8A. In the dark interdendritic areas there is no more fine γ (Fig. 8B) — only small grains with thin light grain boundaries. Perhaps, there was enough deformation of the interdendritic α to cause recrystallization. When the eutectic temperature T_E was reached, the fine γ reacted with α to form liquid eutectic and penetrated the grain boundaries. Upon cooling, the liquid eutectic along the grain boundaries solidified as thin solid eutectic. In fact, as can be seen in the lower-right corner of Fig. 7, similar small grains with thin light grain boundaries and without fine γ are present farther away from the stir zone than the long eutectic films. As mentioned previously, Yamamoto et al. (Refs. 4, 5) proposed that the liquid eutectic films in the stir-zone periphery of AZ91 Mg were engulfed by a growing stir zone and that the liquid eutectic penetrated grain boundaries to cause cracking along the grain boundaries under the torque of the rotating tool. However, it is not clear if the liquid eutectic penetrated the grain boundaries here after the liquid eutectic films had formed first and then been engulfed by a growing stir zone.

Figure 8D is an image taken at point 3 in Fig. 8A. The α dendrite arms and the dark interdendritic areas are both severely elongated along the direction of stirring. Because of the friction heat produced by stirring, the peak temperature should be higher here than at point 1, which is already above T_E. Some fragments of the coarse γ particles might have disappeared after reacting with the interdendritic α and causing further liquation above T_E. Upon cooling, the liquid eutectic along the grain boundaries solidified as solid eutectic. It is interesting to note that the small grains in the elongated interdendritic areas are similar to those in the much less deformed interdendritic areas at Point 2 — Fig. 8C.

Figure 8E is an image taken at point 4 in Fig. 8A. It is similar to that at point 3 — Fig. 8D. However, the dark liquated area is now wider, suggesting more liquation here than at point 3. Few γ particles are left in the upper-left half of the image. Along the grain boundaries in the interdendritic areas, solidified eutectic is visible (α + γ with α connected to the dark interdendritic α). This indicates the presence of liquid eutectic along the grain boundaries. A crack runs along the grain boundaries, suggesting cracking occurred along liquated grain boundaries during FSSW.

Figure 8F shows an image taken at point 5 in Fig. 8A. No γ particles are visible. The dendrite arms and interdendritic areas have mixed with each other to the extent that they are no longer distinguishable. Solid eutectic is present along the

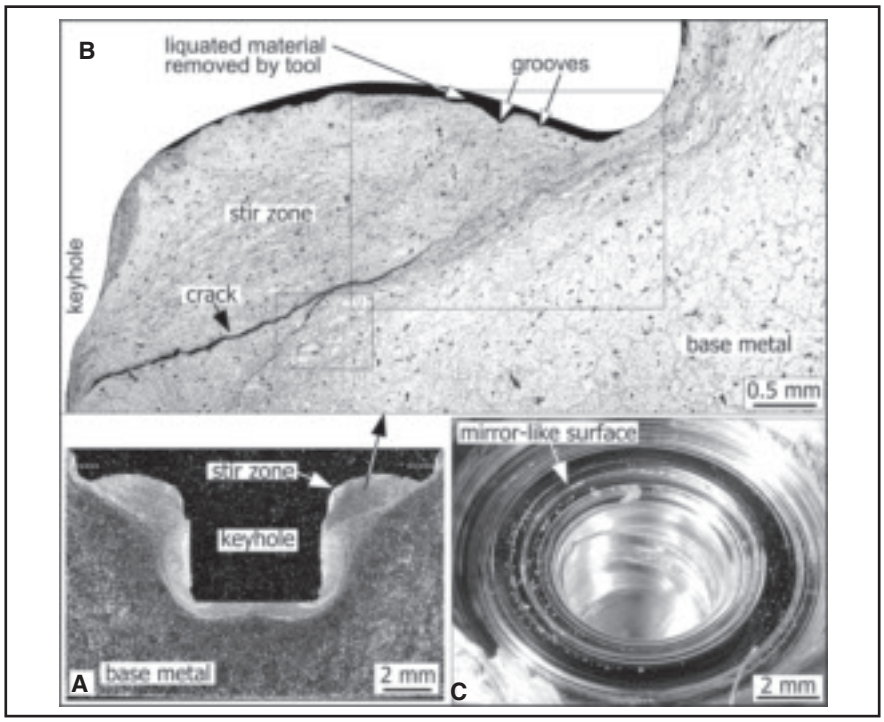

Fig. 6 — Liquation and cracking in weld of as-cast AZ91E Mg. A — Vertical cross section; B — evidence of liquation shown by cracking (small rectangle shown in Fig. 7 and large one Fig. 8A) and removal of liquated material by tool (black area at top of stir zone); C — evidence of liquation shown by mirror-like weld top surface. 15-mm-diameter shoulder, 100- rev/min rotation speed.

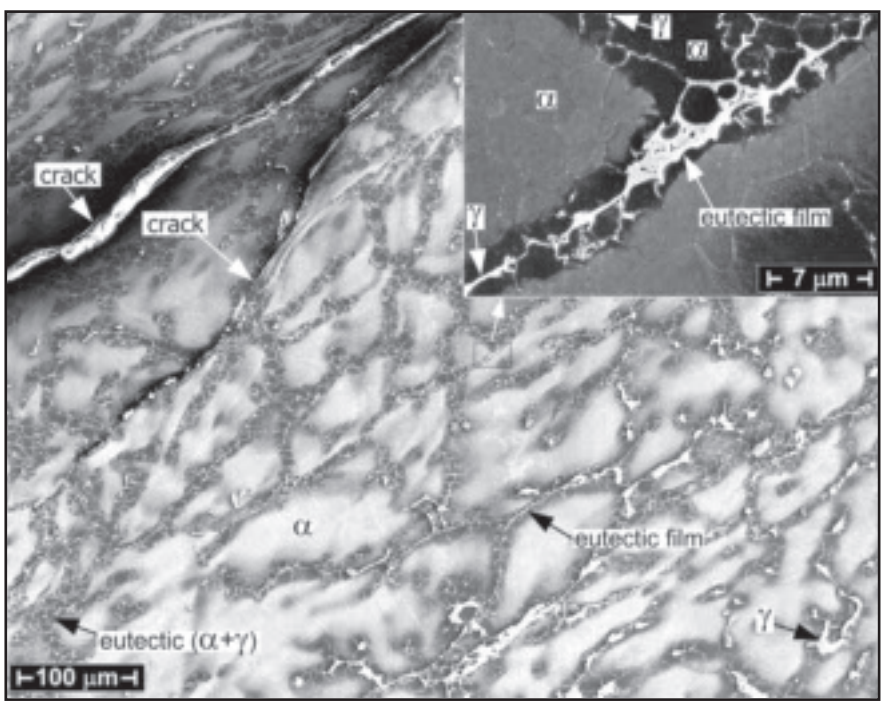

Fig. 7 — SEM image of weld of as-cast AZ91E Mg (small rectangle in Fig. 6B) showing evidence of eutectic liquid films during FSSW. Film enlarged in inset. 15-mm-diameter shoulder, 1000-rev/min rotation speed.

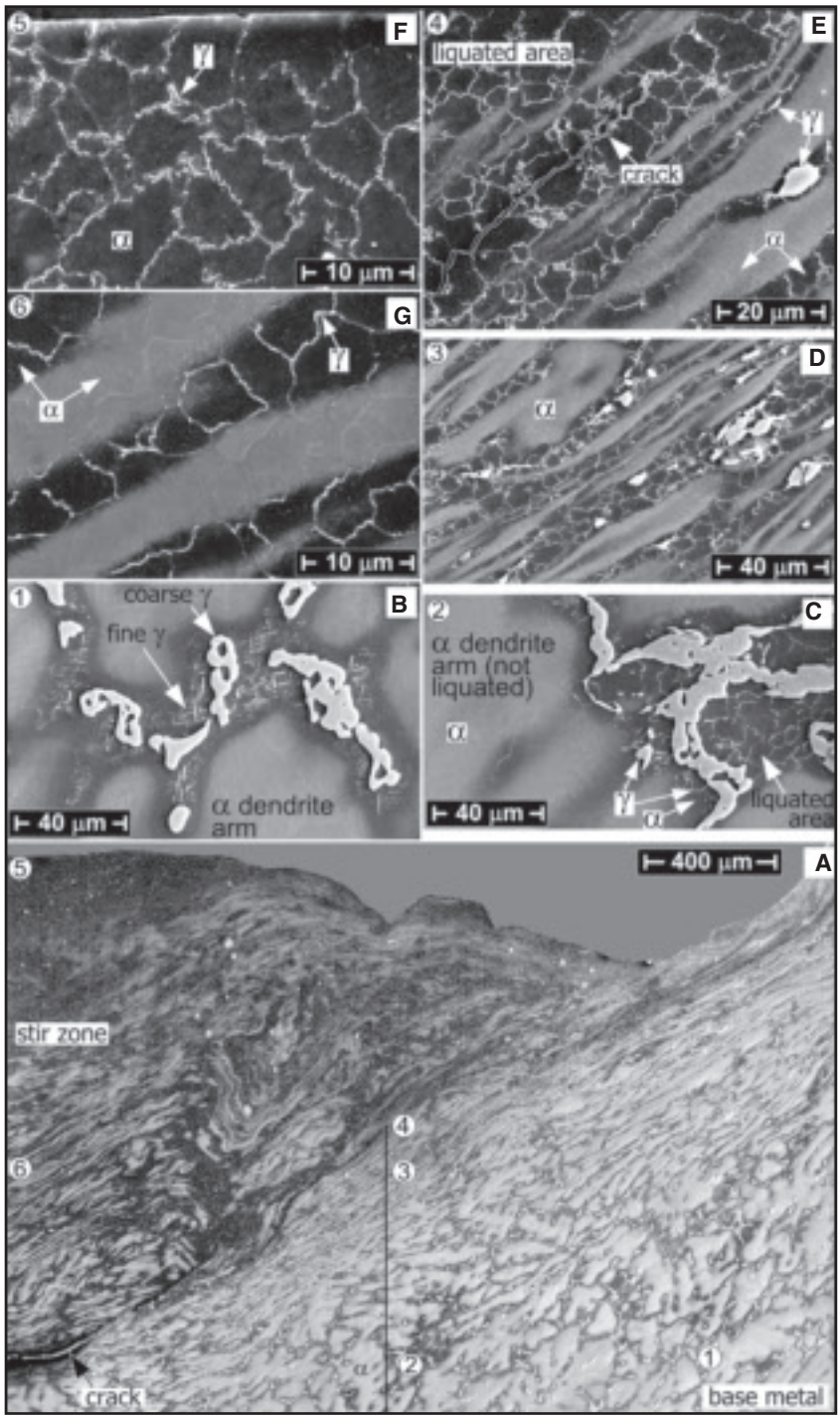

Fig. 8 — SEM images of weld of as-cast AZ91E Mg. A — Vertical cross section (large rectangle in Fig. 6B); B — base metal at point 1 in A; C — liquation at point 2; D — deformation and more liquation at point 3; E — cracking at point 4; F — liquation at point 5; G — liquation at Point 6. 15-mm-diameter shoulder, 1000-rev/min rotation speed.

grain boundaries. It seems that if the material is homogeneous in this area, then there probably is no γ present to react with α and cause liquation by the eutectic reaction $\alpha + \gamma \rightarrow L$. If this is true, liquation near the weld surface could have occurred not by the eutectic reaction but by melting of the α phase at the solidus temperature, that is, by $\alpha \rightarrow L$. Upon cooling to the eutectic temperature the liquid remaining at the grain boundaries can become liquid eutectic and solidify as solid eutectic.

Figure 8G is an SEM image taken at a location similar to that at point 6 in Fig. 8A. No γ particles are visible. Fine grains caused by dynamic recrystallization are present in the α phase both in the dendrites (not clear) and in the interdendritic areas (clear). However, grain-boundary eutectic is present only in the latter.

Microstructural Evolution Leading to Liquation during FSSW

Before proceeding with the microstructural evolution, binary Mg-Al and ternary Mg-Al-Zn phase diagrams are shown first. Figure 9A shows the Mg-rich side of the binary Mg-Al phase diagram (Ref. 22). At the room temperature alloy Mg-8.6Al consists of an α (Mg) matrix and γ ($Mg_{17}Al_{12}$) particles embedded in it. The eutectic reaction $\alpha\,(Mg) + \gamma\,(Mg_{17}Al_{12}) \rightarrow L_E$ occurs at the eutectic temperature T_E of 437°C, where L_E is the liquid eutectic. Figure 9B shows a vertical section (solid lines) of a calculated Mg-Al-Zn ternary phase diagram along which the Al/Zn ratio equals 8.60/0.65 (in wt-%). The vertical section, which is also called an isopleth, includes AZ91E Mg (Mg-8.60Al-0.65Zn if its 0.24 wt-% Mn is ignored as can be seen in Table 1). A calculated binary Mg-Al phase diagram (broken lines) is included for comparison. These two phase diagrams were calculated using the thermodynamic computer code Pandat (Ref. 23) and the database of Mg alloys (Ref. 24). The difference between the two calculated phase diagrams is very small. As shown in Table 1, AZ31 Mg is Mg-3.0Al. AZ91E Mg is approximately Mg-8.6Al if Zn (0.65%) and Mn (0.24%) are ignored. Likewise, AM60 Mg is approximately Mg-6.0Al if Mn (0.5%) is ignored. Thus, the binary Mg-Al phase diagram can be used as an approximation for the vertical section of a ternary Mg-Al-X phase diagram if the content of solute X is small.

The microstructural evolution leading to constitutional liquation in Mg alloys during FSSW is shown in Fig. 10, based on the weld microstructure in AZ91E Mg shown in Fig. 8. Figure 10A is a schematic sketch of the vertical cross section of a weld of alloy C_0 made by FSSW. Alloy C_0 has an abundant γ and a relatively low T_E as most Mg alloys. Figure 10B shows a phase diagram that includes the alloy. It is either a binary Mg-Al phase diagram (Fig. 9A) if the alloy is close to a binary Mg-Al alloy, or a vertical section of a ternary Mg-Al-X phase diagram if the alloy is close to a ternary Mg-Al-X alloy (e.g., Fig. 9B).

The microstructural evolution at a location (point P) heated up to a peak temperature of T_E during FSSW is illustrated in Fig. 10C. At the room temperature T_1 alloy C_0 in its as-cast condition consists of an α matrix and γ particles embedded in it.

The α phase is shown in two different colors — light gray for the dendrite arms and dark gray for the interdendritic area. During casting solute microsegregation causes the liquid to solidify first as α lower in Al ($< C_0$) in the dendrite arms and finally as α higher in Al (up to C_{SM}) and as γ in the interdendritic areas (similar to Fig. 8B).

Because of the high heating rate during FSSW, γ does not have enough time to dissolve in the α phase upon heating to T_2 even though they should do so under the equilibrium (very slow heating) condition according to the phase diagram — Fig. 10B. This is because the solid-state diffusion required for γ dissolution to occur is very slow in view of the very small solid diffusion coefficient (on the order of 1×10^{-8} cm^2/s). The α phase has been deformed by stirring and perhaps some small grains have formed by dynamic recrystallization.

Upon further heating to the eutectic temperature T_E, the remaining γ particles start to react with the surrounding α matrix and cause liquation by the eutectic reaction $\alpha + \gamma \rightarrow L_E$, where L_E is the liquid eutectic — Fig. 10C. This liquation mechanism is the so-called "constitutional liquation" originally observed in fusion welds by Pepe and Savage (Refs. 25, 26). It requires a high heating rate, which usually exists in welding, in order to have γ remain at T_E to react with α and cause liquation. The liquid eutectic penetrates the grain boundaries and solidifies as solid eutectic along the grain boundaries upon cooling.

The microstructural evolution at a location (point Q) heated up to T_3 ($> T_E$) is illustrated in Fig. 10D. Here, α is severely elongated in the direction of stirring, γ breaks up and more liquation occurs. Since bonding between grains can be severely weakened by the presence of liquid, cracking can occur along liquated grain boundaries under the shear force caused by stirring — Fig. 8E. Upon cooling, the liquid eutectic L_E forms solid eutectic S_E along the grain boundaries (similar to Fig. 8D, E).

The microstructural evolution at a location (point R) further up in the stir zone where the material is well mixed is illustrated in Fig. 10E. Here, the peak temperature during FSSW is T_4 ($> T_3 > T_E$). The α dendrites and the interdendritic areas are well mixed and indistinguishable. Upon cooling, the liquid eutectic L_E forms solid eutectic S_E along the grain boundaries (similar to Fig. 8F).

Torque and Axial Force

For a given alloy the tendency to liquate during welding increases with the heat input (Ref. 17). Thus, knowing the heat input in FSSW can help determine whether the difference in the extent of liquation between different alloys is caused by the difference in the heat input or the real susceptibility to liquation. The heat input during FSSW of a given alloy can be affected significantly by its mechanical properties such as the strength. Since the temperature and hence strength vary significantly within the stir zone, it is hard to discuss the heat input based on the strength. An easier way is to analyze the torque and the axial force during FSSW.

Figure 11 shows that both the torque M_z of the rotating tool and the axial force F_z vary with time t and from alloy to alloy. The penetration period lasts for about 42 s and is followed by a 4-s holding period before tool withdrawal. From the torque curve of 6061 Al (Fig. 11A), it can be seen that the rotating tool shoulder reaches the workpiece surface at about 33.5 s. So, the average plunge rate of the 5.1-mm-long pin is about 0.15 mm/s (5.1 mm ÷ 33.5 s), which is identical to the 0.15 mm/s plunge rate used in the experiment. The shoulder plunge lasts for about 8.5 s (42 – 33.5 s). As mentioned previously, the shoulder penetrated only about 0.8 mm below the workpiece surface instead of 1.3 mm (8.5 s × 0.15 mm/s). This difference probably can be accounted for by the very slight workpiece distortion (the resultant workpiece bent downward slightly in the area under the keyhole) and the flexibility in the milling machine system in view of the much (about 7 times) larger cross-sectional area of the shoulder than the pin.

For 6061 Al, a peak torque of about 23 Nm starts to show up at 33.5 s when the rotating tool shoulder reaches the workpiece surface. During the last 4-s holding period, the torque decreases significantly. Initially (t = 0 s), the torque rises quickly and then more slowly as the adjacent workpiece material is heated up and softened by the friction heat produced. It then increases steadily as the tool pin penetrates deeper into the workpiece. As the tool shoulder catches the expelled metal (Fig. 1A), the torque rises quickly again but with fluctuation. The fluctuation is not caused by liquation because of the absence of liquation — Fig. 5. This is likely to be caused by the material expelled by the tool but entrapped between the rotating shoulder and the stationary workpiece surface, which tended to switch back and forth between rotating and stopping.

For AZ91E Mg (Fig. 11B) the torque curve is far below that of 6061 Al, with a maximum torque of only about 10 Nm. No clear peak starts to show up in the torque curve when the rotating tool shoulder reaches the workpiece surface at 33.5 s. The absence of a clear peak torque and the fluctuation of the torque are likely to be caused by liquation. It is likely that when liquid forms, the torque and hence temperature tend to decrease. When the liquid cools and solidifies, the torque and hence temperature increase, and liquid forms again to repeat the cycle.

As shown in Fig. 11, both alloys show two peaks in the curve of axial force F_z vs. time t. The axial force rises quickly initially but decreases as the adjacent workpiece material is heated up and softened. This results in a first peak of about 8 kN in 6061 Al and 7 kN in AZ91E Mg. The axial force rises

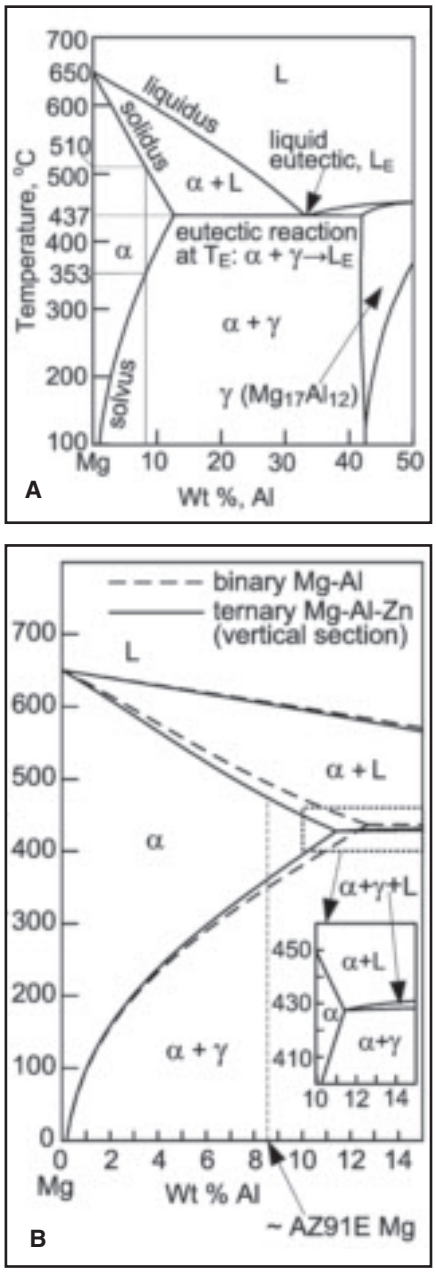

Fig. 9 — Mg phase diagrams. A — Binary Mg-Al phase diagram (Ref. 22); B — vertical section (solid lines, also called isopleth) of Mg-Al-Zn ternary phase diagram at Al/Zn = 8.60/0.65, with a binary Mg-Al phase diagram (broken lines) included for comparison. Both phase diagrams in B calculated using Pandat of CompuTherm LLC (Ref. 23) and Mg database (Ref. 24).

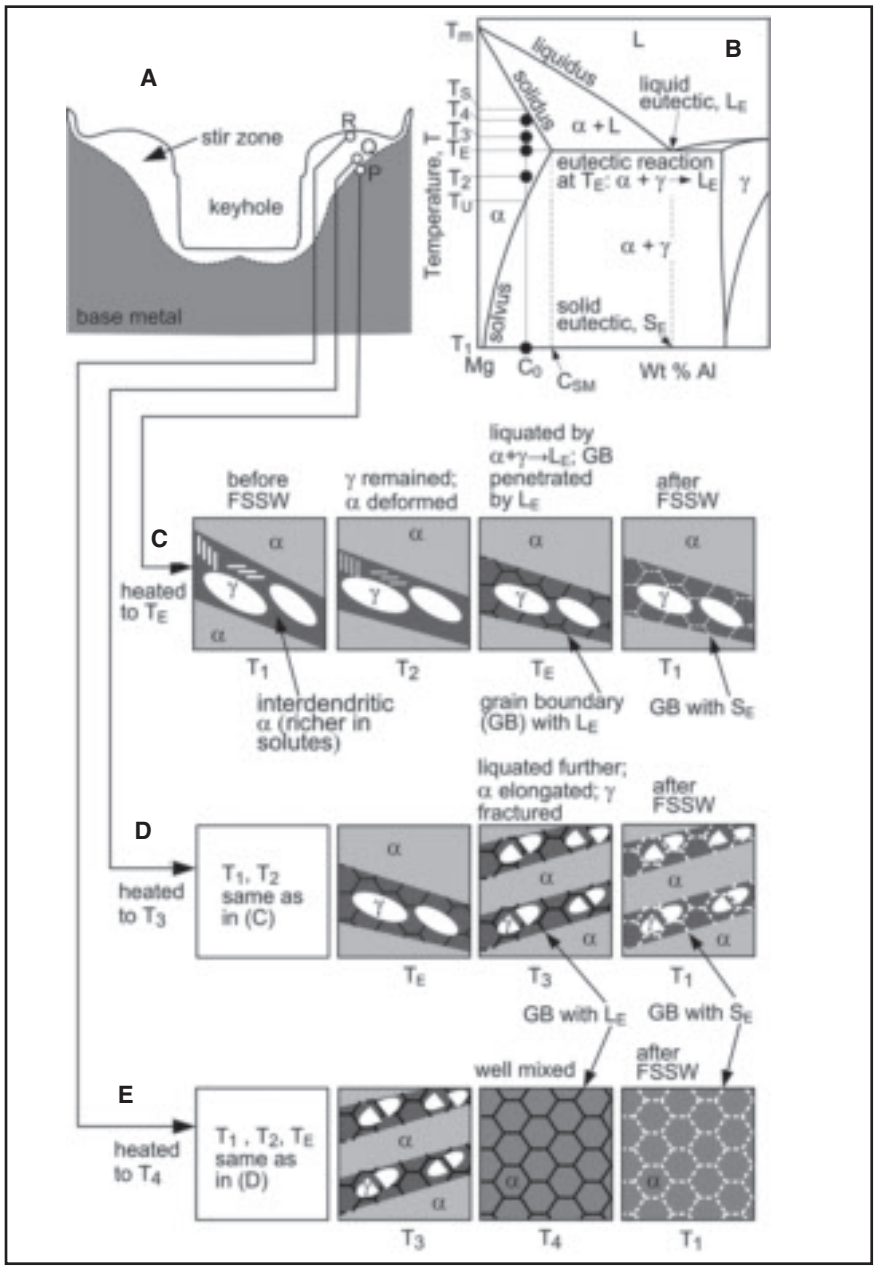

Fig. 10 — Microstructural evolution leading to liquation in FSSW of an alloy with a low eutectic temperature like most Mg alloys. A — Vertical weld cross section; B — phase diagram; C — point P in A (similar to Fig. 8C); D — point Q (similar to Fig. 8D); E — point R (similar to Fig. 8F). Recrystallized grain boundaries in α dendrites (lighter α) not shown.

quickly again as the tool shoulder approaches the workpiece surface. This results in a second peak of about 10 kN in 6061 Al and 15 kN in AZ91E Mg. For 6061 Al, the much lower second peak might be related to its known excellent extrudability. The axial force fluctuated during the same period of time when the torque fluctuated.

Heat Input during FSSW

Let M_z be the torque (in Nm), Ω the rotation speed (in rev/min), and t time (in s). Then the contribution of rotation to the heat input Q_Ω (in Joules) is as follows (Ref. 27):

$$Q_\Omega = \int_0^t M_z \left(\frac{2\pi\Omega}{60}\right) dt \quad (1)$$

Likewise, let F_z be the axial force (in N) and v_z the plunge rate (in m/s). Then, the contribution of tool plunge to the heat input Q_F (in Joules) is as follows (Ref. 28):

$$Q_f = \int_0^t F_z \, v_z \, dt \quad (2)$$

Both the rotation speed Ω and the plunge rate v_Z are often held constant during FSSW. For both materials in the present study, Ω = 1000 rev/min and $v_Z = 1.5 \times 10^{-4}$ m/s. Thus, for constant Ω and v_Z, the total heat input Q due to both tool rotation and plunge in FSSW is as follows:

$$Q = Q_\Omega + Q_F = \left(\frac{2\pi\Omega}{60}\right)\int_0^t M_z \, dt + v_z \int_0^t F_z \, dt \quad (3)$$

The first integral on the right-handside of Equation 3 is the area under the M_Z-t curve. Likewise, the second integral is the area under the F_Z-t curve. As shown in Table 2, the heat input Q_Ω due to tool rotation is 67.5 kJ with 6061 Al and 32.3 kJ with AZ91 Mg. The heat input Q_F due to tool plunge is 35 J with 6061 Al and 51 J with AZ91E Mg. Thus, in FSSW Q_F is much less than Q_Ω. The total heat input Q is 67.5 kJ with 6061 Al and 32.3 kJ with AZ91E Mg, this is consistent with the much lower heat input with AM50 than with 6061 Al observed by Su et al. (Ref. 28).

Thus, the much higher liquation susceptibility of AZ91E Mg in FSSW than 6061 Al cannot be explained by a higher heat input with AZ91E Mg.

Explanation for Liquation Susceptibility in FSSW

A method to explain the liquation susceptibility of an alloy in FSSW is proposed below.

T-f_S Curves and Phase Diagrams

The curve of temperature vs. fraction solid (T-f_S) during solidification shows the eutectic temperature and the amount of the eutectic in an as-cast alloy. The phase diagram also helps identify the liquation-causing constituent in the alloy, for instance, an intermetallic compound in a wrought alloy or a eutectic in an as-cast alloy. In any case, the more abundant the liquation-causing constituent and the lower the liquation temperature, the greater the liquation susceptibility is.

Figure 12 shows the T-f_S curves of AZ31 Mg, AM60 Mg, and AZ91E Mg during solidification. The compositions of these Mg alloys are shown in Table 1. For comparison, the T-f_S curve of 6061 Al is also included as a reference. They were calculated based on the Scheil model using Pandat (Ref. 23) and the solidification databases of Al alloys (Ref. 29) and Mg alloys (Ref. 24). The T-f_S curve for AZ91E Mg has also been calculated by Ohno et al. (Ref. 21) using Pandat and the Mg-alloy database (Ref. 24).

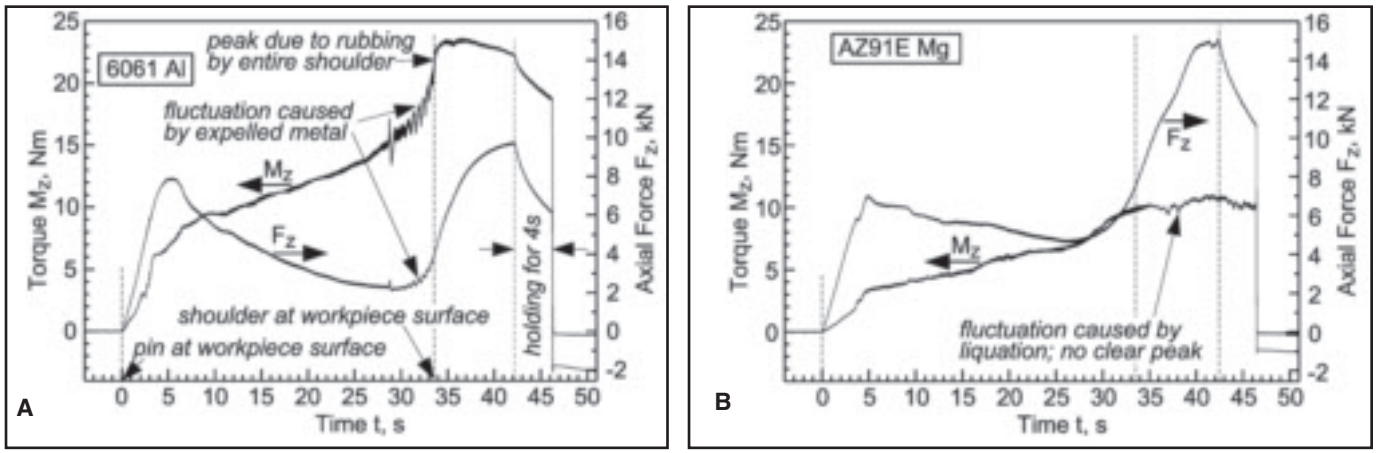

Fig. 11 — Tool torque and axial force measured during FSSW. A — 6061 Al; B — AZ91E Mg. Area under each curve proportional to heat input generated by either rotation (M_Z) or plunge (F_Z) of tool. 15-mm-diameter shoulder, 1000-rev/min rotation speed.

Figure 13 shows the solidus projections of the ternary phase diagrams of Al-Mg-Si (Ref. 30) and (Mg+0.2Mn)-Al-Zn (Ref. 21) on the composition (horizontal) plane. The solidus temperature T_S and the line of solid-solubility limit are shown as a function of composition.

6061 Al

As shown by its T-f_S curve in Fig. 12, 6061 Al does not have much liquation-causing constituent even in the as-cast condition. Even less or none is left after the T6 heat treating. As shown in Table 1, the composition of the 6061 Al used is Al-0.89 Mg-0.62Si-0.52Fe-0.28Cu 0.19Cr 0.08Mn. Fe can be neglected because Fe-rich particles (Fig. 5B) do not cause liquation in 6061 Al (Ref. 14).

AZ91E Mg

According to its T-f_S curve shown in Fig. 12, AZ91E Mg reaches the eutectic reaction $L \rightarrow \alpha + \gamma$ at 432°C and a fraction solid of 0.85, the effect of the low Mn content in this alloy on the curve being negligible. Thus, the AZ91E Mg has a rather high fraction of eutectic of about 15% and a very low eutectic temperature of 432°C, which is 109°C lower than the lowest eutectic temperature of 6061 Al 541°C. This clearly suggests that AZ91E Mg should have a significantly greater tendency to liquate than 6061 Al. The evidence of liquation, cracking, removal of liquated material by the tool, and a mirror-like weld surface shown in Figs. 6 and 7 all confirm the liquation susceptibility of AZ91E Mg.

Other Mg Alloys

Al is the most common alloying element in Mg alloys, and most Mg alloys contain Al as a major alloying element, such as AZ91 Mg, AM60 Mg, and AZ31 Mg, where the first alphabet "A" stands for Al and the first digit for its content (in wt-% and rounded to the closest whole number). As already shown by the Mg-Al phase diagram in Fig. 8A, the eutectic reaction $L \rightarrow \alpha\,(Mg) + \gamma\,(Mg_{17}Al_{12})$ occurs at the eutectic temperature 437°C. Consequently, Mg alloys containing Al tend to liquate at a very low temperature near or even below 437°C.

Figure 12 shows that the Mg alloys have a much lower eutectic temperature and much more eutectic than 6061 Al. The eutectic temperature and the amount of eutectic are 541°C and 1% for 6061 Al, 432°C and 15% for AZ91E Mg, 436°C and 8% for AM60 Mg, and 413°C and 4% for AZ31 Mg.

Thus, it is not surprising that Yamamoto et al. (Ref. 4) observed liquation

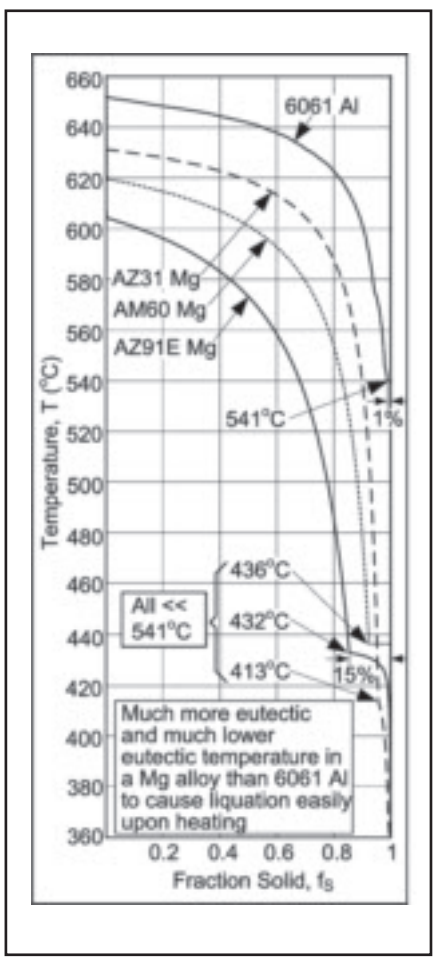

Fig. 12 — T-f_S curves during solidification explaining why Mg alloys are much more liquation susceptible than 6061 Al. Eutectic temperatures and contents: 541°C and 1% for 6061 Al, 432°C and 15% for AZ91E Mg, 436°C and 8% for AM60 Mg, and 413°C and 4% for AZ31 Mg. Curves calculated based on Scheil model of multicomponent alloys using Pandat of CompuTherm LLC (Refs. 21, 23).

Table 2 — Heat Inputs in FSSW

	Heat Input from Rotation Q_Ω (J)	Heat Input from Plunging Q_F (J)	Total Heat Input Q (J)	$\int M_z\,dt$ (Nm s)	$\int Fz\,dt$ (kN s)
6061 Al	67512	35	67547	644.7	232.9
AZ91E Mg	32285	51	32336	308.3	338.3

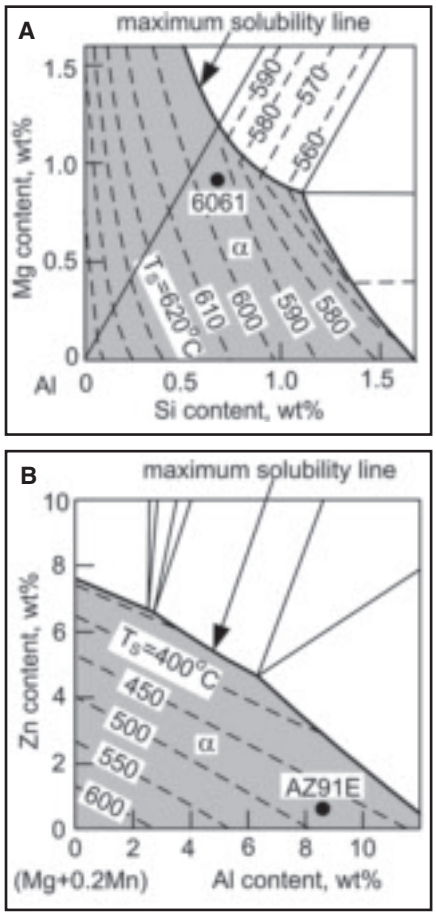

Fig. 13 — Solidus projections showing solidus temperature T_S and line of maximum solubility. A — Ternary Al-Mg-Si in Al (α) corner (Ref. 30); B — ternary (Mg+0.2Mn)-Al-Zn in (Mg+0.2Mn) corner (Ref. 21).

in FSSW of thixomolded AZ91 Mg and AM60 Mg. Liquation was also observed in wrought AZ31 Mg. The extents of liquation were less in wrought AZ31 Mg and thixomolded AM60 Mg than in thixomolded AZ91 Mg. This, in fact, is consistent with the T-f_S curves in Fig. 12, which show less eutectic in the former two Mg alloys. The fact that wrought AZ31 Mg also liquated during FSSW suggests that some liquation-causing constituent still remained after heat treating.

However, with a similar tool and within a wide range of welding conditions including conditions similar to those used for the three Mg alloys, no liquation was observed in 6061 Al (Ref. 7). The higher thermal conductivity of Al alloys can also help conduct heat away from the welding spot into the bulk workpiece and thus reduce the chance of liquation due to over heating. Thus, it is shown that a welding schedule good for a common Al alloy widely used in welding such as 6061 Al may cause liquation in Mg alloys.

Effect of Heat Treating on Liquation Susceptibility

In the binary phase diagram in Fig. 9A, the vertical projection of the solidus line on the horizontal (composition) axis is a line segment. The projection of the solidus plane of a ternary phase diagram on its horizontal (composition) plane, called the solidus projection, is indicated by a shaded area like one of those in Fig. 13. The broken lines within each shaded area indicate how the solidus temperature varies with the composition.

For 6061 Al, as shown by the solidus projection in Fig. 13A, constitutional liquation can occur if liquation-causing constituents are present. Some 6061 Al alloy contains Si-rich particles (Ref. 14), and liquation can occur by the eutectic reaction $\alpha + Si \rightarrow L$ at 577°C or by the eutectic reaction $\alpha + Mg_2Si + Si \rightarrow L$ at 555°C (Ref. 31). Based on the approximate composition of ternary Al-0.9Mg-0.6Si alloy as an approximation and the ternary Al-Mg-Si solidus projection shown in Fig. 13A, it is possible to dissolve all liquation-inducing constituents completely by heat treating at a temperature below the solidus temperature 595°C. Such a 6061 Al can liquate by melting when the solidus temperature 595°C is reached, which is rather high and unlikely to reach in FSSW.

As already shown, constitutional liquation occurs in AZ91E Mg in FSSW. Based on the approximate composition of Mg-8.6Al-0.65Zn-0.2Mn and the ternary (Mg+0.2Mn)-Al-Zn solidus projection shown in Fig. 13B, it is possible to dissolve γ completely by heat treating at a temperature near but below the solidus temperature 475°C. This can raise the liquation temperature from the eutectic temperature 432°C to the solidus temperature 475°C. However, this is still significantly (72°C) lower than the liquation temperature of 6061 Al (541°C), thus suggesting that a heat treated AZ91E Mg can still be more susceptible to liquation. Unfortunately, many Mg alloys are used in the as-cast condition.

A more effective way to reduce the chance of liquation and cracking is to keep the heat input as low as possible (e.g., by using a low rotation speed or a small tool) if welding can be achieved. The weld microstructure can be examined to make sure no liquation or cracking has occurred.

Conclusions

1) Most Mg alloys (e.g., AZ91 Mg, AM60 Mg, and AZ31 Mg) have Al as a major alloying element and they are often used in the as-cast condition, thus providing γ (a $Mg_{17}Al_{12}$ compound containing other alloying elements, e.g., Zn) to react with α (Mg) and cause liquation upon heating by the eutectic reaction $\alpha + \gamma \rightarrow L$ at a low eutectic temperature T_E (e.g., ≤ 437°C).

2) The susceptibility of these Mg alloys to liquation in FSSW is promoted by 1) a liquation-causing constituent γ and a low T_E, and 2) the heat input dwelling at one spot (instead of spreading along the joint path as in FSW).

3) Although Mg is very similar to Al in being light, soft and weldable by FSSW with an alloy-steel tool, a welding schedule good for an Al alloy widely welded by FSSW such as 6061 Al may, in fact, cause liquation in Mg alloys. It is essential to keep the heat input as low as possible and check the weld on liquation and cracking.

4) A liquation-susceptibility test with an augmented torque in FSSW to amplify the difference in liquation between different alloys has been demonstrated, providing not only a simple reliable method for susceptibility testing but also a tool for more clearly examining and understanding liquation.

5) The M_Z-t (torque vs. time) curve can be used to diagnose liquation in real time during FSSW. A curve fluctuating and lacking a clear peak as the rotating tool shoulder reaches and penetrates the workpiece surface indicates likely liquation.

6) A method for explaining the liquation susceptibility in FSSW has been demonstrated, with the T-f_S (temperature vs. fraction solid) curve to indicate T_E and estimate the eutectic content, with the phase diagram to identify the liquation-causing constituent and determine the effect of heat treating, and with the M_Z-t curve to check the heat input.

7) Formation of liquid eutectic films, cracking along liquated grain boundaries, removal of liquated material by the tool, and a mirror-like weld top surface have been observed in AZ91E Mg but not in 6061 Al, thus confirming the liquation susceptibility of AZ91E Mg in FSSW (indicated by the liquation`-susceptibility test) regardless of its much lower heat input (indicated by the torque measurement).

8) The microstructural evolution leading to liquation in FSSW has been presented for alloys with a liquation-causing constituent γ and a low T_E like most Mg alloys.

9) When comparing different alloys in the liquation susceptibility in FSSW, it is desirable to check the heat input in welding each alloy, which can be determined from the M_Z-t curve, because the extent of liquation in a given alloy increases with increasing heat input.

10) Heat treating as-cast Mg alloys before welding may reduce liquation in FSSW by reducing γ, but a more effective way is to keep the heat input as low as possible if there is still enough stirring to achieve sufficient bonding.

Acknowledgments

This work was supported by the National Science Foundation under NSF FRG Grant No. DMR-0605662 and NSF Grant No. DMR-0455484. The authors would like to thank 1) John F. Hinrichs of Friction Stir Link, Inc., Menomonee Falls, Wis., for suggesting the topic of liquation in FSSW for study, 2) Prof. Thomas H. North of University of Toronto, Toronto, Canada, and his former graduate student Adrian P. Gerlich (now assistant professor, University of Alberta, Edmonton, Alberta, Canada) for sharing their publications on FSSW, (3) Prof. Rainer Schmid-Fetzer of Technical University of Clausthal for the Mg database, 4) Prof. Frank Pfefferkorn of University of Wisconsin-Madison and his graduate student Axel Fehrenbacher for assistance in the torque and axial-force measurements, and 5) the reviewers for helpful comments.

References

1. Thomas, W. M., et al. Friction stir butt welding. International Patent Application No. PCT/GB92, Patent Application No. 9125978.8, Dec. 6, 1991.

2. Cao, G., and Kou, S. 2005. Friction stir welding of 2219 aluminum: behavior of θ (Al_2Cu) particles. *Welding Journal* 84: 1-s to 8-s.

3. Gerlich, A., Su, P., and North, T. H. 2005. Peak temperatures and microstructures in aluminum and magnesium alloy friction stir spot welds. *Science and Technology of Welding and Joining* Vol. 10, (6): 647–652

4. Yamamoto, M., Gerlich, A., North , T. H., and Shinozaki, K. 2007. Mechanism of cracking in AZ91 friction stir spot welds. *Science and Technology of Welding and Joining* Vol. 12, (3): 208–216.

5. Yamamoto, M., Gerlich, A., North T. H., and Shinozaki, K. 2007. Cracking in the stir zones of Mg-alloy friction stir spot welds. *Journal of Materials Science* Vol. 42, pp. 7657–7666.

6. Gerlich, A.,Yamamoto, M., and North, T. H. 2007. Local melting and cracking in Al 7075 and Al 2024-T3 friction stir spot welds. *Science and Technology of Welding and Joining*, in press.

7. Gerlich, A. P. 2007. Local Melting and Tool Slippage during Friction Stir Welding of Aluminum Alloys. PhD thesis, Department of Materials Science and Engineering, University of Toronto, Toronto, Ont., Canada.

8. Murr, L. E., Liu, G., and McClure, J. C. 1997. Dynamic recrystallization in friction-stir welding of aluminum alloy 1100. *Journal of Materials Science Letters* 16: 1801–1803.

9. Murr, L. E., Li, Y., Trillo, E. A., Nowak, B. M., and McClure, J. C. 1999. A comparative study of friction-stir welding of aluminum alloys. *Aluminum Transactions* 1: 141–154.

10. Cao, G., and Kou, S. 2006. Predicting and reducing liquation-cracking susceptibility based on temperature vs. fraction solid. *Welding Journal* 85: 9-s to 18-s.

11. Cao, G., and Kou, S. 2005. Liquation cracking in full-penetration Al-Si welds. *Welding Journal* 84: 63-s to 71-s.

12. Huang, C., and Kou, S. 2004. Liquation cracking in full-penetration Al-Cu welds. *Welding Journal* 83: 50-s to 58-s.

13. Huang, C., and Kou, S. 2004. Liquation cracking in full-penetration Al-Mg-Si welds. *Welding Journal* 83: 111-s to 122-s.

14. Huang, C., and Kou, S. 2002. Liquation mechanisms in multicomponent aluminum alloys during welding. *Welding Journal* 81: 211-s to 222-s.

15. Huang, C., and Kou, S. 2001. Partially melted zone in aluminum welds — solute segregation and mechanical behavior. *Welding Journal* 80: 9-s to 17-s.

16. Huang, C., and Kou, S. 2000. Partially melted zone in aluminum welds — liquation mechanism and directional solidification. *Welding Journal* 79: 113-s to 120-s.

17. Kou, S. 2003. *Welding Metallurgy,* 2nd edition, John Wiley and Sons, New York, N.Y., pp. 303–339.

18. The Aluminum Association. 1982. *Aluminum Standards and Data*. p. 15, Washington, D.C., The Aluminum Association.

19. Savage, W. F., and Lundin, C. D. 1965. The Varestraint test. *Welding Journal* 44: 433-s to 442-s.

20. Cao, G., and Kou, S. 2007. Real-Time monitoring of hot tearing in AZ91E magnesium casting. *Transactions of the American Foundry Society,* vol. 115, paper 07-034.

21. Ohno, M., Mirkovic, D., and Schmid-Fetzer, R. 2006. Liquidus and solidus temperature of Mg-Rich Mg-Al-Mn-Zn alloys. *Acta Materialia* 54: 3883–3891.

22. ASM International. 1986. *Binary Alloy Phase Diagrams,* Vol. 1, p. 106, Materials Park, Ohio, ASM International.

23. Pandat — Phase Diagram Calculation software package for Multicomponent Systems. 2001. CompuTherm LLC, Madison, Wis.

24. *PanMagnesium — Thermodynamic Database for Magnesium Alloys*, Computherm LLC, Madison, Wis., 2001, provided by R. Schmidt-Fetzer, Technical University of Clausthal, Institute of Metallurgy, Clausthal-Zellerfeld, Germany.

25. Pepe, J. J., and Savage, W. F. 1967. Effects of constitutional liquation in 18-Ni maraging steel weldment. *Welding Journal* 46(9): 411-s to 422-s.

26. Pepe, J. J., and Savage, W. F. 1970. Weld heat-affected zone of the 18Ni maraging steels. *Welding Journal* 49(12): 545-s to 553-s.

27. Pew, J. W., Nelson, T. W., and Sorensen, C. D. 2007. Torque based weld power model for friction stir welding. *Science and Technology of Welding and Joining*, vol. 12, pp. 341–347.

28. Su, P., Gerlich, A., North, T. H., and Benddzsak, G. J. Energy generation and stir zone dimensions in friction stir spot welds. SAE Technical Series, 2006-01-0971.

29. *PanAluminium — Thermodynamic Database for Commercial Aluminum Alloys*, Computherm LLC, Madison, Wis. 53719, 2001.

30. Philips, H. W. L. 1959. *Annotated Equilibrium Diagrams of Some Aluminum Alloy Systems,* The Institute of Metals, London, pp. 21–86.

31. Mondolfo, L. F. 1976. *Aluminum Alloys Structure and Properties*, pp. 717–857, Boston, Mass., Butterworth.